Anterior-enriched filopodia create appearance of asymmetric membrane microdomains in polarizing *C. elegans* zygotes

Nisha Hirani[1], Rukshala Illukkumbura[1], Tom Bland[1,2], Grégoire Mathonnet[3], Delphine Suhner[3], Anne-Cecile Reymann[3], Nathan W Goehring[1,2,4*]

***For correspondence: nate.goehring@crick.ac.uk (NWG)**

[1]The Francis Crick Institute, 1 Midland Road, London, NW1 1AT, United Kingdom

[2]Institute for the Physics of Living Systems, University College London, London, WC1E 6BT, UK

[3]Institut de Génétique et de Biologie Moléculaire et Cellulaire, Illkirch, Centre National de la Recherche Scientifique, UMR7104, Institut National de la Santé et de la Recherche Médicale, U1258, and Université de Strasbourg, Illkirch, France

[4]MRC Laboratory for Molecular Cell Biology, University College London, Gower Street, London, WC1E 6BT, United Kingdom

JCS Advance Online Article. Posted on 20 June 2019

ABSTRACT

The association of molecules within membrane microdomains is critical for the intracellular organization of cells. During polarization of the *C. elegans* zygote, both polarity proteins and actomyosin regulators associate within dynamic membrane-associated foci. Recently, a novel class of asymmetric PIP_2 membrane-associated structures was described, suggesting that PIP_2 domains could constitute signaling hubs to promote cell polarization and actin nucleation. Here we probe the nature of these domains using a variety of membrane- and actin cortex-associated probes. These data demonstrate that these domains are filopodia, which are stimulated transiently during polarity establishment and accumulate in the zygote anterior. The resulting membrane protrusions create local membrane topology that quantitatively accounts for observed local increases in fluorescence signal of membrane-associated molecules, suggesting molecules are not selectively enriched in these domains relative to bulk membrane and that the PIP_2 pool as revealed by $PH_{PLC\delta1}$ simply reflects plasma membrane localization. Given the ubiquity of 3D membrane structures in cells, including filopodia, microvilli, and membrane folds, similar caveats are likely to apply to analysis of membrane-associated molecules in a broad range of systems.

SUMMARY STATEMENT

Apparent accumulation of PIP_2 and cortex/polarity-related proteins within plasma membrane microdomains in polarizing C. elegans zygotes reflects local membrane topology induced by filopodia, not selective enrichment within signaling domains.

INTRODUCTION

Micro- to nano-scale heterogeneity in the distribution of proteins and lipids in the plasma membrane has emerged as a fundamental organizing principle of the cell (***Simons and Ikonen, 1997***; ***Balla, 2013***; ***Schink et al., 2016***; ***Stone et al., 2017***). By partitioning molecules into distinct compartments, local clustering can also serve a potentially powerful mechanism for regulating molecular behavior.

During polarity establishment of the *C. elegans* zygote, clustering of a conserved set of PAR proteins (PAR-3, PAR-6, and PKC-3) on the membrane is critical for their ability to be segregated into the nascent anterior by actomyosin cortical flows (***Rodriguez et al., 2017***; ***Wang et al., 2017***; ***Dickinson et al., 2017***), eventually allowing them to be replaced by a second opposing set of PAR proteins (PAR-1, PAR-2, LGL-1 and CHIN-1) on the posterior membrane (***Rose and Gonczy, 2014***; ***Goehring, 2014***). Cortical flows are in turn controlled by local foci of RHO-1 activation, which drive pulsatile actin nucleation and contraction of the cortical actomyosin network (***Nishikawa et al., 2017***; ***Michaux et al., 2018***) (Summarized in Figure 1A).

Asymmetric enrichment of $PI(4,5)P_2$, hereafter PIP_2, has been observed within another class of membrane-associated domains in the anterior of the *C. elegans* zygote (***Nakayama et al., 2009***; ***Wang et al., 2017***; ***Scholze et al., 2018***). Similar enrichment is seen for the polarity-related Rho-family GTPases CDC-42 and RHO-1, the RHO-1 regulator ECT-2, a CDC-42-associated sub-population of PAR-6 and PKC-3, and casein kinase (CSNK-1) (***Motegi and Sugimoto, 2006***; ***Schonegg et al., 2007***; ***Panbianco et al., 2008***; ***Wang et al., 2017***). PIP_2-enriched microdomains have been proposed to serve as organizing platforms to coordinate regulation of cortical actin organization, cell polarity, and asymmetric division of the zygote (***Scholze et al., 2018***). Despite being noted over a decade ago, the nature of these domains remains poorly understood.

RESULTS

Diverse membrane-associated molecules appear co-enriched in membrane structures

To reveal the nature of these domains, we confirmed previous results that polarity-related proteins RHO-1, CDC-42, and CSNK-1 colocalized to a similar class of membrane-associated domains labeled by the PIP_2 probe, $PH_{PLC\delta1}$ in *C. elegans* zygotes. All proteins labeled similar domains, which varied with the cell cycle, peaked during polarity establishment, and colocalized with >90% of PIP_2-labeled domains (***Nakayama et al., 2009***; ***Motegi and Sugimoto, 2006***; ***Schonegg et al., 2007***; ***Panbianco et al., 2008***; ***Scholze et al., 2018***) (Figure 1B, Figure S1, S2). Given this coincidence, we determined whether co-labeling was specific. We therefore co-expressed $PH_{PLC\delta1}$ with various plasma membrane markers, including the syntaxin, SYX-4 (***Jantsch-Plunger and Glotzer, 1999***), a myristoylated form of mKate, $mKate_{myr}$, and the plasma membrane protein EGG-1 (***Kadandale et al., 2005***). Surprisingly, all proteins marked >90% of $PH_{PLC\delta1}$-labeled domains (Figure 1B-E). To further control for non-specific labeling of bulk plasma membrane, we examined localization of the membrane dye FM4-64, which also labeled >90% of $PH_{PLC\delta1}$-positive domains (Figure 1B, F, Movie S1). We observed quantitative agreement in the relative enrichment of $PH_{PLC\delta1}$ and FM4-64 signal within domains, indicating that there is no selective enrichment of molecules, including of PIP_2, within these domains relative to bulk membrane.

Polarizing embryos exhibit asymmetric filopodia-like structures

What could be the origin of these $PH_{PLC\delta1}$-labeled domains that could explain their non-specific labeling by membrane-associated molecules? A clue came from observations of extended tubular structures protruding from the cell that were evocative of filopodia, which were particularly evident near the pseudocleavage furrow where the membrane pulls away from the eggshell (Figure 2A).

Filopodia are thin, dynamic, actin-rich membrane protrusions. Their formation and extension is driven by actin polymerization downstream of Arp2/3 and formins and is regulated by actin-regulatory molecules including actin bundling and capping proteins (***Mattila and Lappalainen, 2008***), with Myosin-X and formins typically enriched at their tips (***Jacquemet et al., 2019***). Because there is no homologue of Myosin-X in *C. elegans*, we examined localization of the embryonically-expressed formin CYK-1 co-expressed with red fluorophore fusions to $PH_{PLC\delta1}$ or $mKate_{myr}$ (***Swan et al., 1998***). CYK-1 was enriched at the tips of extended tubular structures and comet-like structures at the cortex (Figure 2A-B, Figure S3A and Movies S2, S3). We interpret the latter structures to be the same as extended tubular structures but pressed against

the embryo surface by the eggshell. Intercalating CYK-1-tipped finger-like projections were also observed at regions of cell-cell contacts at both 2- and 4-cell stages (Figure 2C). CYK-1 puncta were distinct from large pulsatile foci that are also present during the polarity establishment phase (Figure 2B*, K*) and which have been shown to coincide with pulsatile actomyosin (***Michaux et al., 2018***).

CYK-1-tipped structures were dynamic, exhibiting processive motion across the plasma membrane at velocities consistent with prior quantification of filopodia growth rates (***Argiro et al., 1985***) (Figure 2D, E). To further establish the filopodia-like nature of these structures, we examined LifeAct::GFP, which extensively co-localized with mCherry:: $PH_{PLC\delta1}$ signal in putative filopodia and appeared to extend throughout filopodia-like structures (Figure 2F-H, Movie S4). We also found that >80% of filopodia-like structures were labeled by the *C. elegans* ortholog of the actin bundling protein plastin (PLST-1 in *C. elegans,* ***Ding et al.*** (***2017***)) (Figure 2I, Figure S3A, B), consistent with data from other systems (***Jacquemet et al., 2019***). Finally, the combined loss of both CYK-1 and ARP-2/3 function prevented their formation (Figure S3C), consistent with prior work demonstrating the dependence of PIP_2 domains on actin (***Scholze et al., 2018***). By contrast, loss of either cortical contractility or PAR polarity did not affect the formation of filopodia, only their asymmetry along the anterior-posterior axis (Figure S3D).

Numbers of CYK-1 puncta generally correlated with appearance of $PH_{PLC\delta1}$-labeled structures (Figure 2J-K, Movie S5): Numbers of both were initially low, peaking after the transition to maintenance phase, which coincides with reorganization of the actin cortex (Figure 2J-K, 0 sec) (***Munro et al., 2004***; ***Velarde et al., 2007***). Both then declined and remained largely absent until reappearing at the onset of cytokinesis (Figure 2J-K, 400-500 sec). This correlation suggests that filopodia account for the vast majority of $PH_{PLC\delta1}$-labeled structures in the zygote.

Preferential labeling of distinct F-actin populations by different LifeAct probes

The co-localization we observe between LifeAct::GFP and $PH_{PLC\delta1}$ differed from previous work in which PIP_2 enrichment was reported to precede LifeAct::mKate enrichment by nearly 10 seconds (***Scholze et al., 2018***). We wondered whether the divergent results were due to employment of differently tagged versions of LifeAct. Co-expression of both GFP and mKate versions of LifeAct in embryos revealed distinct localization behaviors. Most noticeably, LifeAct::mKate appeared to segregate preferentially into the anterior (Figure 3A,C) and was unequally inherited by the anterior daughter cell (AB) relative to its sister P1 and again by the P1 daughter EMS relative to its sister P2 (Figure 3B). Neither behavior was observed

for LifeAct::GFP. LifeAct::mKate also poorly labeled posterior structures that were labeled efficiently by LifeAct::GFP (Figure 3A).

LifeAct::GFP and LifeAct::mKate also showed distinct labeling of filopodia. Whereas LifeAct::GFP efficiently labeled dynamic filopodia extending from the cell, LifeAct::mKate was depleted (Figure 3D). LifeAct::mKate also lagged behind LifeAct::GFP in filopodia moving along the embryo surface and in cytoplasmic actin comets (Figure 3E-H, Movie S6, S7). Finally, we observed a gap between CYK-1 puncta at filopodia tips and LifeAct::mKate signal, consistent with a lag in labeling filopodia (Figure 3I-J).

Lags in actin probe localization have been associated with slow turnover rates in the context of actin flow (e.g. LifeAct vs. Utrophin, (***Bement et al., 2015***; ***Maiuri et al., 2015***)). LifeAct is generally thought to turn over rapidly, but behavior can vary with fluorophore and expression level (***Riedl et al., 2008***; ***Spracklen et al., 2014***; ***Courtemanche et al., 2016***; ***van der Honing et al., 2011***). We therefore used fluorescence recovery after photobleaching (FRAP) to analyze the binding kinetics (Figure 3K-L). LifeAct::mKate turnover rates were an order of magnitude slower than for LifeAct::GFP ($r_{1/2}$ = 21.6 ± 8.9 vs 0.84 ± 0.27 s), reaching time scales comparable to turnover of cortical F-actin in the *C. elegans* cortex (***Robin et al., 2014***). We conclude that slow turnover of LifeAct::mKate leads to its localization to a discrete, potentially more stable or long-lived sub-population of actin structures, which explains the previously observed lag in LifeAct::mKate localization to PIP_2-labeled structures (***Scholze et al., 2018***). The temporal lag we observe matches the reported delay between $PH_{PLC\delta1}$ and LifeAct::mKate (10 vs 9.3 s). Consistent with this interpretation, artificially stabilizing LifeAct::GFP at the membrane by co-expression with a membrane-tethered GFP-binding protein induced segregation of LifeAct::GFP, reproducing the segregation phenotype to observed with LifeAct::mKate (Figure 3M). Affinity differences in LifeAct probes could also potentially explain reported resistance of cortical actin to actin-disrupting agents in LifeAct::mKate-expressing lines relative to prior work (***Goehring et al., 2011***; ***Michaux et al., 2018***; ***Scholze et al., 2018***).

Membrane topology quantitatively accounts for local 'enrichment' of membrane-associated molecules

But how could filopodia result in apparent local enrichment of membrane-associated molecules? One possibility is that enrichment simply reflects the local accumulation of membrane within ruffles, tubes, or folds within the imaging plane, increasing local fluorescence above the surrounding single membrane bilayer. This effect, described previously in mammalian cells, would occur even if protein concentration

on the membrane was uniform (***van Rheenen and Jalink, 2002***)

To determine whether locally increased signal could be explained by membrane topology, we compared the distribution of fluorescence of mCherry::$PH_{PLC\delta1}$ obtained by confocal microscopy with what would be expected if membrane concentration were uniform, but a filopodia was immediately adjacent to the membrane. To this end, we obtained z-stacks of embryos expressing mCherry::$PH_{PLC\delta1}$ during the establishment phase. Bright spots were visible in individual planes which could be assigned to filopodia in 3-D renderings (Figure 4A, arrowheads). These filopodia were brighter than regions containing a single membrane bilayer, but less bright than the double membrane bilayer of the pseudocleavage furrow (Figure 4A, arrows). Quantification of experimental intensities were then compared to those obtained from a simulated image, which was constructed by assuming the presence of a single 5 nm-thick bilayer, flanked by a second bilayer in the region of the pseudocleavage furrow, and a 100 nm diameter filopodium, assuming uniform membrane concentration (Figure 4C-D, see Methods). Intensity distributions were remarkably similar, with experimental measurements almost exactly matching predictions from simulated images (Figure 4E-F).

Thus, for the molecules analyzed here, including PIP_2, RHO-1, CDC-42, and CSNK-1, local cortical signal in filopodia-like structures can be fully explained by changes in local membrane topology, arguing against any concentration of these molecules within micron-scale domains in the plasma membrane or asymmetric enrichment of PIP_2 in the zygote anterior. While filopodia are the dominant features underlying this phenomenon in the zygote, any local changes in membrane topology would present similar problems, including membrane ruffles, folds, or protrusions, making this a widespread issue for quantification of local membrane concentration.

It is noteworthy that despite similar asymmetry of anterior structures, only CDC-42, which is known to interact with anterior-enriched PAR proteins, exhibited pronounced polarity when quantified in cross-section and retained this asymmetric enrichment during maintenance phase when filopodia dissipated, arguing against overall asymmetry of either PIP_2 or RHO-1 (Figure S4). One should also note that the localization of activity sensors for CDC-42 and RHO-1 tend not to match localization of the proteins overall (***Nishikawa et al., 2017***; ***Kumfer et al., 2010***), consistent with local regulation of activity, rather than local accumulation alone, being critical for localized function of these GTPases. Anterior PIP_2 enrichment is also difficult to reconcile with observations that the PI4K kinase, PPK-1, is modestly enriched in the embryo posterior, opposite to what would be expected if high PIP_2 levels defined the anterior (***Panbianco et al., 2008***), and LGL and PAR-2 are both thought to rely on PIP_2 for membrane association, despite being enriched in the posterior (***Motegi et al., 2011***; ***Dong et al., 2015***). We therefore favor a global, rather than

local, role for PIP_2, which is consistent with the sensitivity of the zygote to bulk changes in PIP_2 levels that was recently reported (***Scholze et al., 2018***).

The existence of PIP_2 membrane domains remains controversial (***van Rheenen and Jalink, 2002***; ***Stone et al., 2017***; ***van den Bogaart et al., 2011***; ***Wang and Richards, 2012***; ***Ji et al., 2015***). While we cannot rule out the existence of PIP_2 membrane domains that are not revealed by the probes used to date, in light of our data, we feel there is currently no compelling experimental evidence to support the existence of PIP_2 microdomains or anterior PIP_2 enrichment in the *C. elegans* zygote.

METHODS AND MATERIALS

Strains, growth, and media

C. elegans strains were maintained on nematode growth media (NGM) under standard conditions (***Brenner, 1974***) at 16°C or 20°C unless otherwise indicated. Strains are listed in Table S1.

Strain construction

$mKate_{myr}$ consists of the first 11 AA of SRC-2 harboring the N-myristoylation site, followed by a 3xMyc tag, mKate, and the coding sequence of iLID (***Guntas et al., 2015***). The coding sequence is expressed under the *mex-5* promoter and *nmy-2* 3'UTR in plasmid pNG17, which was introduced by biolistic bombardment into DP38 worms creating strain NWG0045 (***Praitis et al., 2001***). SWG19 was generated by backcrossing SWG4 (***Reymann et al., 2016***) to N2 (4x).

RNAi

RNAi was performed according to described methods (***Kamath et al., 2003***). Briefly, HT115(DE3) bacterial feeding clones were inoculated from LB agar plates to LB liquid cultures and grown overnight at 37°C in the presence of 10 µg/ml carbenicillin. 100 µl of bacterial cultures was spotted onto 60 mm agar RNAi plates (10 µg/ml carbenicillin, 1 mM IPTG). L4 larva were added to RNAi feeding plates and incubated for 20-48 hrs depending on gene and temperature. RNAi clones targeting *arx-2*, *ect-2*, *par-2*, *perm-1*, *pkc-3*, and *wve-1* were obtained from the Ahringer library, which is currently available via Source BioScience (Nottingham, UK).

Embryo dissection and mounting

For imaging, embryos were typically dissected in egg buffer (118 mM NaCl, 48 mM KCl, 2mM $CaCl_2$, 2mM $MgCl_2$, 25 mM HEPES pH 7.4) or M9 and mounted under a 2 or 3% agarose pad and sealed with VALAP (1:1:1, Vaseline, lanolin, paraffin wax). For FM4-64 experiments, *perm-1(RNAi)* embryos were dissected and mounted in 0.75% egg buffer, with 18-20 µm beads (Polysciences, Warrington, PA, USA) under a coverslip, and two edges sealed with VALAP to create a flow chamber (***Carvalho et al., 2011; Goehring et al., 2011***). FM4-64 (5 µg/ml in 0.75% egg buffer) was then introduced by capillary action.

Microscopy and image acquisition

Confocal Image Acquisition

Midsection images were captured on a Nikon TiE with a 100x 1.45 N.A. objective, further equipped with a custom X-Light V1 spinning disk system (CrestOptics, Rome, Italy) with 50 μm slits, Obis 488/561 fiber-coupled diode lasers (Coherent, Santa Clara, CA, USA) and an Evolve Delta EMCCD camera (Photometrics, Tuscon, AZ, USA). Imaging systems were run using Metamorph (Molecular Devices, San Jose, CA, USA) and configured by Cairn Research (Kent, UK). Filter sets were from Chroma (Bellows Falls, VT, USA): ZT488/561rpc, ZET405/488/561/640X, ET525/50m, ET630/75m, ET655LP.

Surface confocal images were acquired with spinning disk confocal microscope every 2 s (CYK-1: Zeiss C-Apochromat with Yokogawa CSU-X1 scan head, Orca-Flash4.0 camera (Hamamatsu Photonics, Japan), 100X/1.42 NA, and run using Micro-Manager; PLST-1: Inverted Nikon Eclipse Ti equipped with Yokogawa CSU-X1 scan head, simultaneous dual camera with two Prime 95B cameras (Photometrics), 100X 1.4 NA objective, configured by Gataca Systems (Massy, France) and run using Metamorph.

Hilo Imaging

Unless otherwise specified, surface images were captured by HiLo microscopy (***Konopka and Bednarek, 2008***; ***Tokunaga et al., 2008***) on a Nikon TiE with 100x N.A. 1.49 objective, further equipped with a iLAS TIRF unit (Roper, Lisse, France), custom field stop, Obis 488/561 fiber-coupled diode lasers (Coherent) and an Evolve Delta. Imaging systems were run using Metamorph and configured by Cairn Research. Filter sets were from Chroma: ZT488/561rpc, ZET488/561x, ZET488/561m, ET525/50m, ET630/75m, ET655LP. FRAP was performed in a 6.2 x 6.2 µm box in the anterior of maintenance phase embryos with 20 prebleach frames and an imaging interval of 0.5 s.

Data Analysis

Image processing and data analysis were performed in Python (www.python.org), Matlab (Mathworks, Natick, MA, USA), and Fiji (***Schindelin et al., 2012***). For statistical comparisons, all data points are shown and significance assessed using a Students t-test, two-tailed.

FRAP

FRAP analysis was performed in Matlab using scripts provided in ***Goehring et al.*** (***2010***), but fit to a single exponential to extract $\tau_{1/2}$.

CYK-1 tracking

Filopodia tip velocity measurements were obtained by tracking CYK-1::GFP puncta, which was performed in Python using the *trackpy* package (https://github.com/soft-matter/trackpy). Custom Python code developed for the analysis is available at https://github.com/lhcgeneva/SPT. Briefly, a Crocker-Grier algorithm detects local intensity peaks, which are then fit to a Gaussian point spread function with the detection threshold adjusted empirically for imaging conditions. An independently acquired dataset was quantified using the MOSAIC plugin in Fiji (http://mosaic.mpi-cbg.de/?q=downloads/imageJ) together with custom Matlab codes for data analysis to confirm results.

Spatial/temporal fluorescence profiles

In general, fluorescence profiles (both experimental and simulated) were obtained by tracking a 3-pixel wide line along the membrane from images subjected to a Gaussian Blur (σ = 1 px) to reduce noise. Mean normalized profiles after subtraction of chip background were extracted and plotted in Matlab.

For Figure 3G, clear filopodia-like structures were identified that were isolated from other structures that would complicate analysis. After obtained fluorescence profiles along filopodia in both channels, data from each filopodium was aligned based on the peak of GFP::LifeAct intensity.

For Figure 3H, fluorescence profiles along the path of the actin comets were obtained overtime and the data plotted as a two-channel kymograph. Temporal change was calculated across a minimum of ten spatial positions for each individual comet, the resulting data aligned by the time of peak GFP fluorescence, before averaging to obtain the average temporal profile of GFP and mKate for each comet. $\Delta\tau$ was defined as the peak to peak time difference between maximal GFP and mKate accumulation calculated from average

temporal profiles of each comet.

For Figure 3K, profiles of LifeAct::mKate and $PH_{PLC\delta1}$ relative to CYK-1 puncta were obtained by first identifying clear filopodia with comet-like morphologies from a minimum of 3 embryos each. A 3-pixel line beginning at the center of the CYK-1 focus and running through the PH / LifeAct labeled region was then defined and straightened in Fiji. Fluorescence profiles were then extracted in Matlab, normalized to mean intensity and plotted as a function of distance from CYK-1 puncta at the filopodia tip.

For quantification of relative peak intensities in Figure 1I and 4F, 3-pixel wide profiles across membrane features were extracted, cytoplasmic background subtracted, and the top three peak intensity pixels summed. Data was normalized to median intensities obtained in regions of the plasma membrane devoid of membrane structures representing a single bilayer configuration in the same embryo. Simulated images were treated identically except that they were normalized to the median value of all single membrane peaks.

Colocalization

Regions of interest (ROIs) were manually defined for a minimum of 30 well-defined and separated structures in the reference channel for each embryo, usually using the channel showing fluorescent protein fusions to $PH_{PLC\delta1}$. ROIs were then queried in the test channel to score whether the structure was labeled by the other molecule, scoring either for the presence of a similar structure, or a tip-localized punctum in the case of CYK-1. The fraction of structures showing co-localization was calculated for each embryo.

Asymmetry index

For Figure 3C, the asymmetry index (ASI) of cortical LifeAct was calculated by first obtaining mean fluorescence values from selected regions of the cell cortex in the anterior and posterior halves of the zygote in background subtracted images. We then calculated ASI according to the equation $ASI = (A-P)/(2(A+P))$, where A and P are the fluorescence values in the anterior and posterior, respectively. The resulting ASI range from -0.5 to 0.5, with 0 being symmetric, and -0.5 and 0.5 being maximally polarized towards posterior or anterior, respectively.

In Figure S4, ASI was calculated from membrane intensity profiles around the circumference of the embryo extracted from cross-sectional confocal images. Briefly, a 50-pixel wide line following the membrane around the embryo was computationally straightened and a normalized cytoplasmic GFP curve was subtracted to isolate membrane signal following the procedure in ***Reich et al.*** (***2019***). Mean intensity values corresponding to the posterior and anterior regions of the embryo (each representing 1/3 of total

circumference) were then used to calculate ASI as above.

Image simulations

To simulate fluorescence microscopy images of hypothesized experimental membrane configurations, a starting image of resolution 5 nm/px was generated to match the dimensions of the experimental image in Figure 4B. The membrane bilayer was simulated as a 1-pixel wide line, which was used to trace the hypothesized membrane configuration from the experimental image. This included a region containing part of the pseudocleavage furrow, which generates a double membrane as well as a circle 100 nm in diameter to mimic the cross section of the filopodial membrane. A uniform background level of photons was added before subjecting the resulting image to a 200 nm wide Guassian blur and resampling to the experimental resolution of 0.155 µm/px. Modulated Poisson noise and readout noise (5 standard deviations) was then added before processing identically to the experimental image. All manipulations were performed in Fiji.

Competing interests

The authors declare no competing interests.

Author Contributions

Conceptualization, A.C.R., N.W.G.; Methodology, N.H, R.I., T.B.; Formal Analysis: R.I., T.B., A.C.R., N.W.G.; Investigation, N.H., R.I., T.B., G.M., D.S., A.C.R., N.W.G.; Resources, N.H., G.M., D.S.; Writing – original draft preparation, N.W.G.; Writing – review and editing, All authors; Funding Acquisition, A.C.R., N.W.G.; Supervision, A.C.R., N.W.G.

Funding

This work was supported by the Francis Crick Institute (NWG), which receives its core funding from Cancer Research UK (FC001086), the UK Medical Research Council (FC001086), and the Wellcome Trust (FC001086), the EU Horizon 2020 research and innovation programme under the Marie Skłodowska-Curie grant agreement 675407 (to NWG), the initiative of excellence IDEX-Unistra (ANR-10-IDEX-0002-02) from the French national programme "Investment for the future" (to ACR) and the grant ANR-10-LABX-

0030-INRT, a French State fund managed by the Agence Nationale de la Recherche under the frame program Investissements d'Avenir ANR-10-IDEX-0002-02 (to ACR). GM is an IGBMC International PhD Programme fellow supported by LabEx INRT funds. Some imaging was supported by the Imaging Center of IGBMC (ici.igbmc.fr) with assistance from Elvire Guiot, Erwan Grandgirard and Bertrand Vernay. NWG and ACR are members of the GENiE network supported by COST Action BM1408 and EMBO. Some strains were provided by the CGC, which is funded by NIH Office of Research Infrastructure Programs (P40 OD010440).

REFERENCES

Argiro V, Bunge MB, Johnson MI. (1985). A quantitative study of growth cone filopodial extension. *Journal of Neuroscience Research*. 13(1-2):149–62.

Audhya A, Hyndman F, McLeod IX, Maddox AS, Yates JR, Desai A, Oegema K. (2005). A complex containing the Sm protein CAR-1 and the RNA helicase CGH-1 is required for embryonic cytokinesis in *Caenorhabditis elegans*. *The Journal of Cell Biology*. 171(2):267–279.

Balla T. (2013). Phosphoinositides: Tiny Lipids With Giant Impact on Cell Regulation. *Physiological Reviews*. 93(3):1019–1137.

Bement WM, Leda M, Moe AM, Kita AM, Larson ME, Golding AE, Pfeuti C, Su KC, Miller AL, Goryachev AB, von Dassow G. (2015). Activator–inhibitor coupling between Rho signalling and actin assembly makes the cell cortex an excitable medium. Nature Cell Biology. 17(11):1471–1483.

van den Bogaart G, Meyenberg K, Risselada HJ, Amin H, Willig KI, Hubrich BE, Dier M, Hell SW, Grubmüller H, Diederichsen U, Jahn R. (2011) Membrane protein sequestering by ionic protein–lipid interactions. Nature. 479:552.

Brenner S. (1974) The genetics of *Caenorhabditis elegans*. Genetics. 77(1):71–94.

Carvalho, A, Olson, SK, Gutierrez, E, Zhang, K, Noble, LB, Zanin, E, Desai, A, Groisman, A, and Oegema, K. (2011) Acute drug treatment in the early *C. elegans* embryo. PLoS One. *6*, e24656.

Courtemanche N, Pollard TD, Chen Q. (2016) Avoiding artefacts when counting polymerized actin in live cells with LifeAct fused to fluorescent proteins. Nature Cell Biology. 18(6):676–683.

Cuenca AA, Schetter A, Aceto D, Kemphues K, Seydoux G. (2003) Polarization of the *C. elegans* zygote proceeds via distinct establishment and maintenance phases. Development (Cambridge, England). 130(7):1255–1265.

Dickinson DJ, Schwager F, Pintard L, Gotta M, Goldstein B. (2017) A Single-Cell Biochemistry Approach Reveals PAR Complex Dynamics during Cell Polarization. Developmental Cell. 42(4):416–434.

Ding WY, Ong HT, Hara Y, Wongsantichon J, Toyama Y, Robinson RC, Nédélec F, Zaidel-Bar R. (2017) Plastin increases cortical connectivity to facilitate robust polarization and timely cytokinesis. Journal of Cell Biology. 216(5):1371-1386.

Dong W, Zhang X, Liu W, Chen Yj, Huang J, Austin E, Celotto AM, Jiang WZ, Palladino MJ, Jiang Y, Hammond GRV, Hong Y. (2015) A conserved polybasic domain mediates plasma membrane targeting of Lgl and its regulation by hypoxia. The Journal of Cell Biology. 211(2):273–86.

Goehring NW. (2014) PAR polarity: From complexity to design principles. Experimental Cell Research. 328(2):258–266.

Goehring NW, Chowdhury D, Hyman AA, Grill SW. (2010) FRAP Analysis of Membrane-Associated Proteins: Lateral Diffusion and Membrane-Cytoplasmic Exchange. Biophysical Journal. 99(8):2443–2452.

Goehring NW, Hoege C, Grill SW, Hyman AA. (2011) PAR proteins diffuse freely across the anterior–posterior boundary in polarized *C. elegans* embryos. The Journal of Cell Biology. 193(3):583–594.

Guntas G, Hallett RA, Zimmerman SP, Williams T, Yumerefendi H, Bear JE, Kuhlman B. (2015) Engineering an improved light-induced dimer (iLID) for controlling the localization and activity of signaling proteins. Proceedings of the National Academy of Sciences of the United States of America. 112(1):112–117.

van der Honing HS, van Bezouwen LS, Emons AMC, Ketelaar T. (2011) High expression of Lifeact in *Arabidopsis thaliana* reduces dynamic reorganization of actin fiaments but does not affect plant development. Cytoskeleton. 68(10):578–587.

Jacquemet G, Stubb A, Saup R, Miihkinen M, Kremneva E, Hamidi H, Ivaska J. (2019) Filopodome Mapping Identifies p130Cas as a Mechanosensitive Regulator of Filopodia Stability. Current Biology. 29(2):202–216.

Jantsch-Plunger V, Glotzer M. (1999) Depletion of syntaxins in the early *Caenorhabditis elegans* embryo reveals a role for membrane fusion events in cytokinesis. Current Biology. 9(14):738–745.

Ji C, Zhang Y, Xu P, Xu T, Lou X. (2015) Nanoscale landscape of phosphoinositides revealed by specific pleckstrin homology (PH) domains using single-molecule superresolution imaging in the plasma membrane. Journal of Biological Chemistry. 290(45):26978–26993.

Jordan SN, Davies T, Zhuravlev Y, Dumont J, Shirasu-Hiza M, Canman JC. (2016) Cortical PAR polarity proteins promote robust cytokinesis during asymmetric cell division. Journal of Cell Biology. 212(1):39–49.

Kachur TM, Audhya A, Pilgrim DB. (2008) UNC-45 is required for NMY-2 contractile function in early embryonic polarity establishment and germline cellularization in *C. elegans*. Developmental Biology. 314(2):287–299.

Kadandale P, Stewart-Michaelis A, Gordon S, Rubin J, Klancer R, Schweinsberg P, Grant BD, Singson A. (2005) The egg surface LDL receptor repeat- containing proteins EGG-1 and EGG-2 are required for fertilization in *Caenorhabditis elegans*. Current Biology. 15(24):2222–2229.

Kamath RS, Fraser AG, Dong Y, Poulin G, Durbin R, Gotta M, Kanapin A, Le Bot N, Moreno S, Sohrmann M, Welchman DP, Zipperlen P, Ahringer J. (2003) Systematic functional analysis of the *Caenorhabditis elegans* genome using RNAi. Nature. 421(6920):231–237.

Konopka CA, Bednarek SY. (2008) Variable-angle epiflorescence microscopy: A new way to look at protein dynamics in the plant cell cortex. Plant Journal. 53(1):186-96.

Kumfer KT, Cook SJ, Squirrell JM, Eliceiri KW, Peel N, O'Connell KF, White JG. (2010) CGEF-1 and CHIN-1 Regulate CDC-42 Activity during Asymmetric Division in the *Caenorhabditis elegans* Embryo. Molecular Biology of the Cell. 21(2):266–277.

Maiuri P, Rupprecht JF, Wieser S, Ruprecht V, Bénichou O, Carpi N, Coppey M, De Beco S, Gov N, Heisenberg CP, Lage Crespo C, Lauten- schlaeger F, Le Berre M, Lennon-Dumenil AM, Raab M, Thiam HR, Piel M, Sixt M, Voituriez R. (2015) Actin Flows Mediate a Universal Coupling between Cell Speed and Cell Persistence. Cell. 161(2):374–386.

Mattila PK, Lappalainen P. (2008) Filopodia: molecular architecture and cellular functions. Nature reviews Molecular cell biology. 9(6):446–54.

Michaux JB, Robin FB, McFadden WM, Munro EM. (2018) Excitable RhoA dynamics drive pulsed contractions in the early *C. elegans* embryo. The Journal of Cell Biology. 217(12):4230-4252.

Motegi F, Sugimoto A. (2006) Sequential functioning of the ECT-2 RhoGEF, RHO-1 and CDC-42 establishes cell polarity in *Caenorhabditis elegans* embryos. Nature Cell Biology. 8(9):978–985.

Motegi F, Zonies S, Hao Y, Cuenca AA, Griffin EE, (2011) Seydoux G. Microtubules induce self-organization of polarized PAR domains in *Caenorhabditis elegans* zygotes. Nature Cell Biology. 13(11):1361–1367.

Munro E, Nance J, Priess JR. (2004) Cortical flows powered by asymmetrical contraction transport PAR proteins to establish and maintain anterior-posterior polarity in the early *C. elegans* embryo. Developmental Cell. 7(3):413–424.

Nakayama Y, Shivas JM, Poole DS, Squirrell JM, Kulkoski JM, Schleede JB, Skop AR. (2009) Dynamin participates in the maintenance of anterior polarity in the *Caenorhabditis elegans* embryo. Developmental Cell. 16(6):889–900.

Neukomm LJ, Zeng S, Frei AP, Huegli PA, Hengartner MO. (2014) Small GTPase CDC-42 promotes apoptotic cell corpse clearance in response to PAT-2 and CED-1 in *C. elegans*. Cell Death and Differentiation. 21(6):845–853.

Nishikawa M, Naganathan SR, Jülicher F, Grill SW. (2017) Controlling contractile instabilities in the actomyosin cortex. eLife. 6:1–21.

Panbianco C, Weinkove D, Zanin E, Jones D, Divecha N, Gotta M, Ahringer J. (2008) A Casein Kinase 1 and PAR Proteins Regulate Asymmetry of a PIP2 Synthesis Enzyme for Asymmetric Spindle Positioning. Developmental Cell.15(2):198–208.

Praitis V, Casey E, Collar D, Austin J. (2001) Creation of low-copy integrated transgenic lines in *Caenorhabditis elegans*. Genetics. 157(3):1217–26.

Redemann S, Pecreaux J, Goehring NW, Khairy K, Stelzer EHK, Hyman AA, Howard J. (2010)

Membrane Invaginations Reveal Cortical Sites that Pull on Mitotic Spindles in One-Cell *C. elegans* Embryos. PLoS ONE. 5(8):e12301.

Reich JD, Hubatsch L, Illukkumbura R, Peglion F, Bland T, Hirani N, Goehring NW. (2019) Regulated activation of the PAR polarity network ensures a timely and specific response to spatial cues. Current Biology. (in press).

Reymann AC, Staniscia F, Erzberger A, Salbreux G, Grill SW. (2016) Cortical flow aligns actin filaments to form a furrow. eLife. 5:e17807.

van Rheenen J, Jalink K. (2002) Agonist-induced PIP(2) hydrolysis inhibits cortical actin dynamics: regulation at a global but not at a micrometer scale. Molecular Biology of the Cell. 13(9):3257–67.

Riedl J, Crevenna AH, Kessenbrock K, Yu JH, Neukirchen D, Bista M, Bradke F, Jenne D, Holak TA, Werb Z, Sixt M, Wedlich-Soldner R. (2008) Lifeact: a versatile marker to visualize F-actin. Nature methods. 5(7):605–7.

Robin FB, McFadden WM, Yao B, Munro EM. (2014) Single-molecule analysis of cell surface dynamics in *Caenorhabditis elegans* embryos. Nature Methods. 11(6):677–682.

Rodriguez J, Peglion F, Martin J, Hubatsch L, Reich J, Hirani N, Gubieda AG, Roffey J, Fernandes AR, St Johnston D, Ahringer J, Goehring NW. (2017) aPKC Cycles between Functionally Distinct PAR Protein Assemblies to Drive Cell Polarity. Developmental Cell. 42(4):400–415.

Rose L, Gonczy P. (2014) Polarity establishment, asymmetric division and segregation of fate determinants in early *C. elegans* embryos. WormBook. 1-43.

Schindelin J, Arganda-Carreras I, Frise E, Kaynig V, Longair M, Pietzsch T, Preibisch S, Rueden C, Saalfeld S, Schmid B, Tinevez JY, White DJ, Hartenstein V, Eliceiri K, Tomancak P, Cardona A (2012) Fiji: An open source platform for biological image analysis. Nature Methods. 9(7):676–682.

Schink KO, Tan KW, Stenmark H. (2016) Phosphoinositides in Control of Membrane Dynamics. Annual Review of Cell and Developmental Biology. 32(1):143–171.

Scholze MJ, Barbieux KS, De Simone A, Boumasmoud M, Süess CCN, Wang R, Gönczy P. (2018) PI(4,5)P2 forms dynamic cortical structures and directs actin distribution as well as polarity in *Caenorhabditis elegans* embryos. Development. 145(11):dev164988.

Schonegg S, Constantinescu AT, Hoege C, Hyman AA. (2007) The Rho GTPase-activating proteins RGA-3 and RGA-4 are required to set the initial size of PAR domains in *Caenorhabditis elegans* one-cell embryos. Proceedings of the National Academy of Sciences of the United States of America. 104(38):14976–14981.

Simons K, Ikonen E. (1997) Functional rafts in cell membranes. Nature. 387(6633):569–572.

Spracklen A J, Fagan TN, Lovander KE, Tootle TL. (2014) The pros and cons of common actin labeling tools for visualizing actin dynamics during *Drosophila* oogenesis. Developmental Biology. 393(2):209–226.

Stone MB, Shelby SA, Veatch SL. (2017) Super-Resolution Microscopy: Shedding Light on the Cellular Plasma Membrane. Chemical Reviews. 117(11):7457–7477.

Swan KA, Severson AF, Carter JC, Martin PR, Schnabel H, Schnabel R, Bowerman B. (1998) *cyk-1*: a *C. elegans* FH gene required for a late step in embryonic cytokinesis. Journal of Cell Science. 11:2017-2027.

Tokunaga M, Imamoto N, Sakata-Sogawa K. (2008) Highly inclined thin illumination enables clear single-molecule imaging in cells. Nature Methods. 5(2):159-161.

Velarde N, Gunsalus KC, Piano F. (2007) Diverse roles of actin in *C. elegans* early embryogenesis. BMC Developmental Biology. 7(1):142.

Wang J, Richards DA. (2012) Segregation of PIP2 and PIP3 into distinct nanoscale regions within the plasma membrane. Biology Open. 1(9):857–862.

Wang SC, Low TYF, Nishimura Y, Gole L, Yu W, Motegi F. (2017) Cortical forces and CDC-42 control clustering of PAR proteins for *Caenorhabditis elegans* embryonic polarization. Nature Cell Biology. 19(8):988–995.

Zonies S, Motegi F, Hao Y, Seydoux G. (2010) Symmetry breaking and polarization of the *C. elegans* zygote by the polarity protein PAR-2. Development (Cambridge, England). 137(10):1669–1677.

Figures

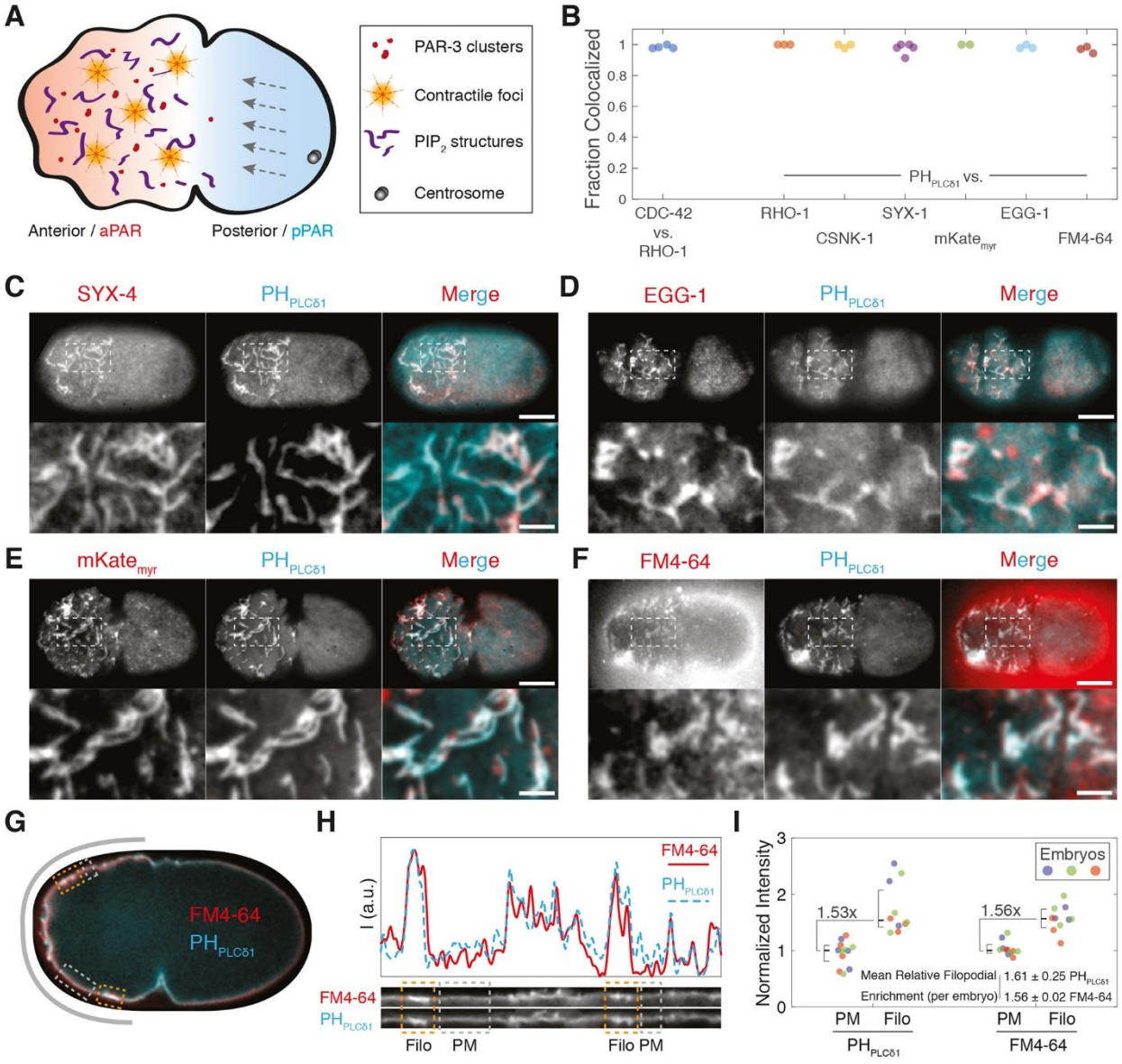

Figure 1. Diverse membrane-associated molecules co-label common membrane structures.

(A) Schematic of *C. elegans* zygote polarization, highlighting PAR-3 clusters, contractile foci, and putative PIP_2-enriched membrane domains. Polarization of PAR proteins (red/blue) is induced by anterior-directed actomyosin cortical flows (grey arrows).

(B) Fraction of membrane structures co-labeled by indicated markers. Sample images in (C-F), Figure S2.

(C-F) Surface images of embryos expressing FP-tagged $PH_{PLC\delta1}$ with transmembrane syntaxin, SYX-4

(GFP::SYX-4) **(C)**, oocyte-enriched membrane protein EGG-1 (GFP::EGG-1) **(D)**, a myristoylated form of mKate, $mKate_{myr}$ **(E)**, and membrane dye FM4-64 **(F)**. Individual channels and merge shown (whole embryo and inset zoom). Scale bar, 10 µm (embryo), 2.5 µm (inset).

(G) Cross-section of embryo expressing GFP-tagged $PH_{PLC\delta1}$ with FM4-64 (n = 3). Boxes highlight plasma membrane (grey, PM) and filopodia (orange, Filo). Grey band indicates region straighten in (H).

(H) A 20-pixel wide straightened region taken along the indicated path in (G). $PH_{PLC\delta1}$ and FM4-64 shown individually with normalized intensity plots. Orange and grey boxes highlight regions marked in (G).

(I) Fluorescence intensity for PM and Filo regions from embryos co-labeled with $PH_{PLC\delta1}$ and FM4-64. Intensity normalized to embryo median (color coded) with overall median ± 95% CI shown for all datapoints. Relative median filopodia enrichment between probes is indicated. Mean relative filopodia enrichment ± SD of individual embryo means is also provided.

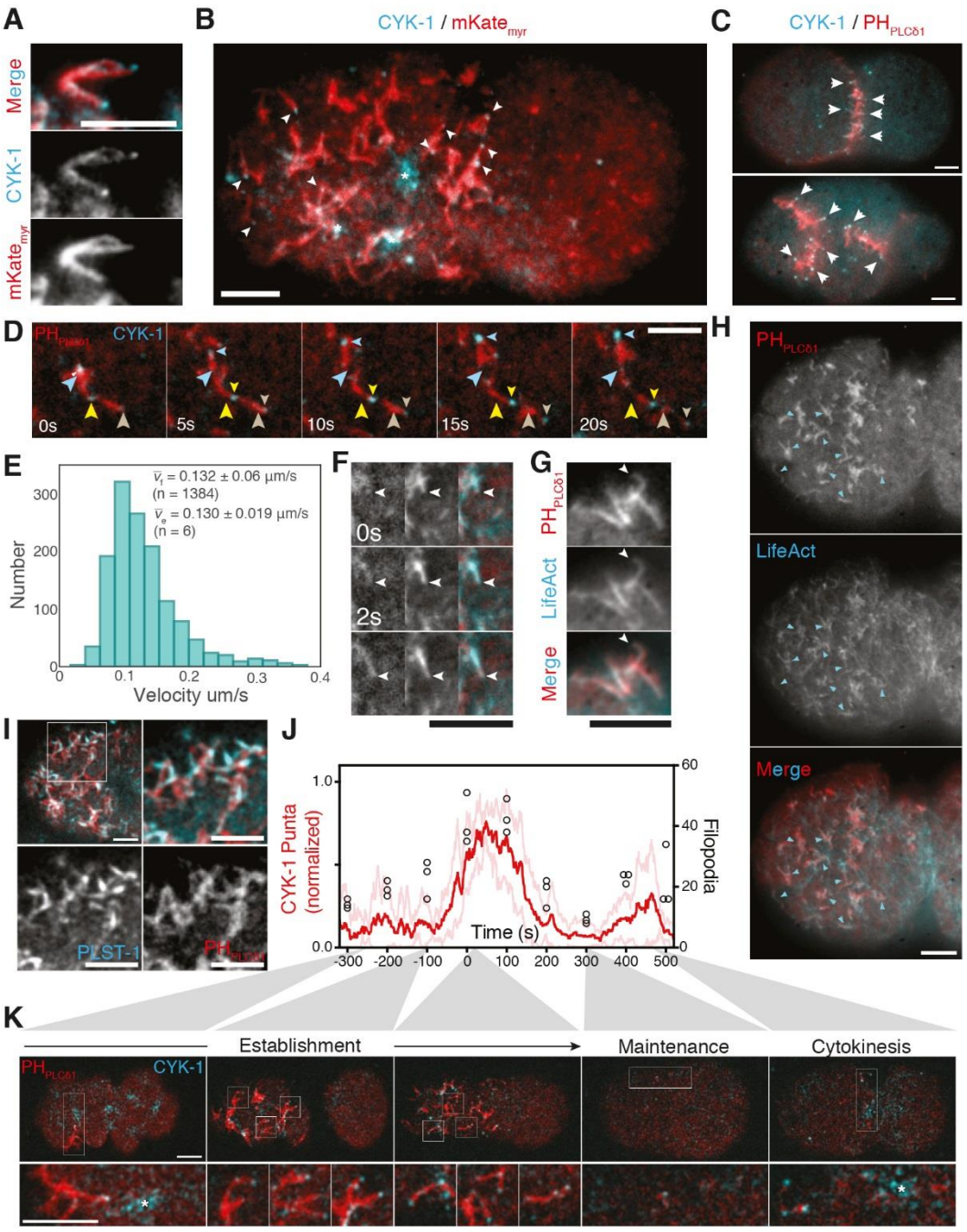

Figure 2. Asymmetric cortical structures resemble filopodia.

(A) Magnified region from the pseudocleavage furrow in embryo expressing mKate$_{myr}$ and CYK-1::GFP. See Movie S2.

(B) CYK-1 localization to large contractile foci (*), and tips of mKate$_{myr}$-labeled filopodia-like structures revealed by mKate$_{myr}$ (arrowheads) in embryo anterior.

(C) Surface images of 2- and 4-cell embryos expressing CYK-1::GFP and mCherry::$PH_{PLC\delta1}$. Arrowheads mark CYK-1-tipped membrane structures at cell contacts.

(D) Timecourse of filopodia movement. Large arrowheads denote CYK-1::GFP puncta at time = 0s. Position in subsequent frames marked by small arrowheads. See Movie S3.

(E) Histogram of CYK-1::GFP puncta velocities. v_f denotes mean velocity ± SD for all CYK-1 puncta. v_e is the mean of embryo means.

(F) Growth timecourse of a single filopodium from embryo in (H) highlighting LifeAct localization throughout the extending structure (mCherry::$PH_{PLC\delta1}$, left, LifeAct::GFP, middle, merge, right). See Movie S4.

(G) Example of LifeAct::GFP labeling throughout extended mCherry::$PH_{PLC\delta1}$-positive filopodia. Labeling observed in 13/13 extended filopodia (3 embryos).

(H) Extensive colocalization of LifeAct::GFP with mCherry::$PH_{PLC\delta1}$ within putative filopodia (n = 4).

(I) Cortical image of embryo anterior showing mCherry::$PH_{PLC\delta1}$ and PLST-1::GFP (top left). Boxed inset magnified (top right) with individual channels shown below. Quantification, additional images in Figure S3A, B.

(J) Number of CYK-1 puncta (normalized to peak number, mean (red) ± SD (pink)) and $PH_{PLC\delta1}$-labeled structures (black circles) over time. Time = 0 sec is the transition between establishment and maintenance phase marked by relaxation of the pseudocleavage furrow. Cytokinesis is between 400-500 sec.

(K) Confocal cortical images of embyro expressing CYK-1::GFP and mCherry::$PH_{PLC\delta1}$ at representative timepoints. Insets marked, shown magnified 3x below. *indicates large pulsatile foci common at polarity establishment and cytokinesis. See Movie S5. Colocalization of CYK-1 puncta with mCherry::$PH_{PLC\delta1}$-labeled structures in Figure S3A.

Scale bars, 5 µm.

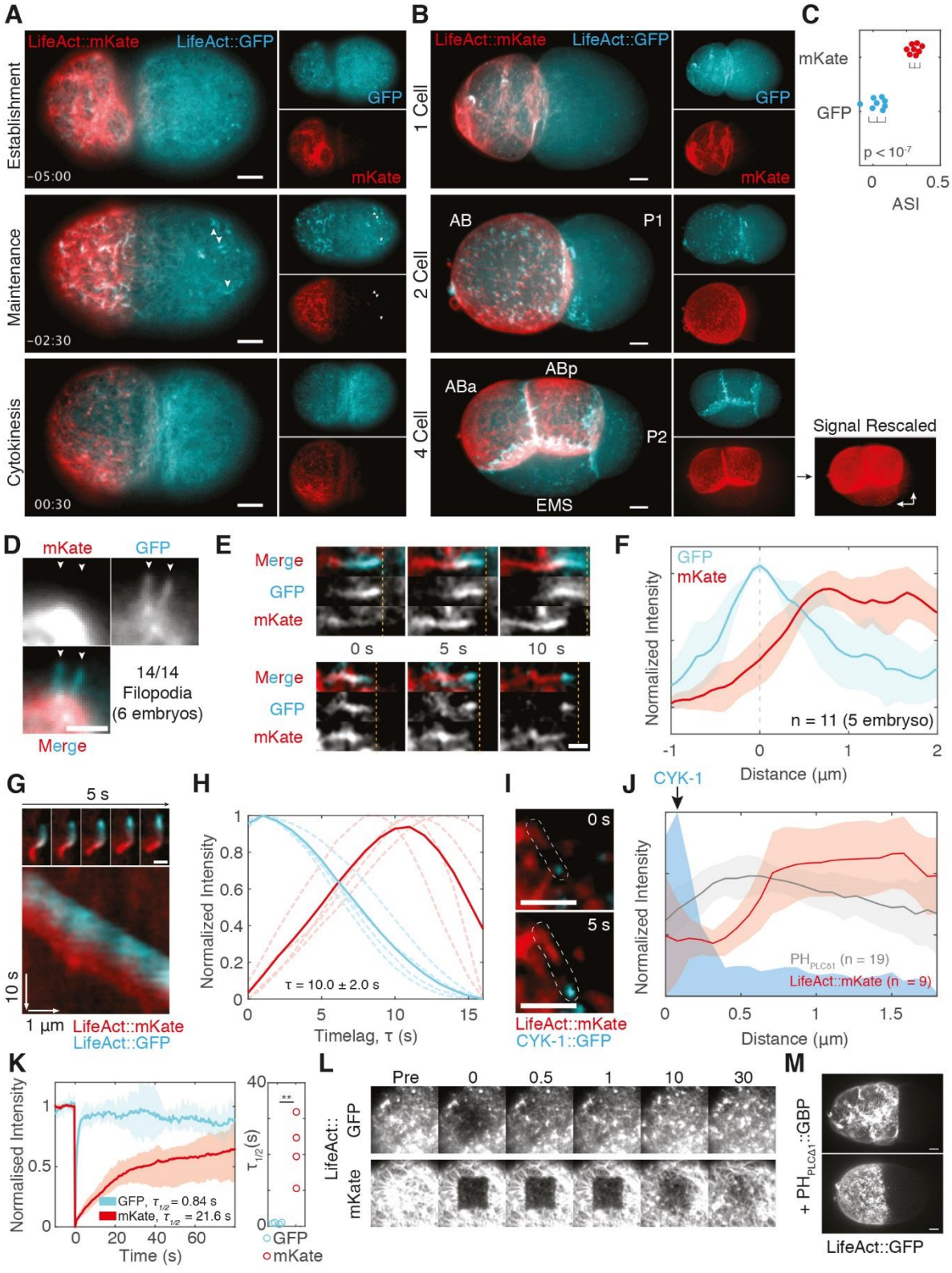

Figure 3. LifeAct::GFP and LifeAct::mKate label distinct actin populations *in vivo*.

(A) Cortical images of LifeAct::mKate vs. LifeAct::GFP during the first cell cycle, quantified in (C). Arrowheads mark posterior filopodial structures that are only labeled by LifeAct::GFP. Time (min:sec) relative to cytokinesis.

(B) Max 3D projections of 1-, 2- and 4-cell embryos. LifeAct::mKate signal in the 4-cell embryo is shown rescaled to highlight asymmetry between EMS and P2 (arrows)

(C) Asymmetry (ASI) of LifeAct::GFP vs. LifeAct::mKate signal in 1-cell establishment phase embryos (panel A).

(D) LifeAct::GFP, but not LifeAct::mKate, labels filopodia extending from the cell surface.

(E) LifeAct::mKate lags LifeAct::GFP labeling of two processive surface-associated filopodia. Computationally straightened images shown. Dashed lines mark leading edge of GFP signal for reference. See Movie S6.

(F) Lag of LifeAct::mKate relative to peak LifeAct::GFP signal in fluorescence intensity traces along filopodia.

(G) Timelapse images of a cytoplasmic actin comet labeled with LifeAct::mKate and LifeAct::GFP and an associated kymograph taken along a trace of the comet path. See Movie S7.

(H) Quantification of LifeAct::mKate time lag measured from kymographs as in (G). Average temporal change across a minimum of ten positions for each individual comet (n=4) shown along with mean of embryo means. $\Delta\tau$ is the peak to peak time lag.

(I) Timelapse of filopodia labeled by CYK-1::GFP and LifeAct::mKate.

(J) Quantification of LifeAct::mKate or mCherry::$PH_{PLC\delta1}$ relative to GFP::CYK-1 puncta. Mean ± SD shown.

(K) FRAP analysis of cortical LifeAct::GFP vs. LifeAct::mKate following bleaching of a 6.2x6.2 µm box. Mean FRAP trace ± max/min (left) shown along with $\tau_{1/2}$ for each replicate. **p<0.01, t-test, two-tailed.

(L) Timeseries of FRAP experiments in (K).

(M) Stabilization of LifeAct::GFP by membrane-tethered GFP nanobody ($PH_{PLC\delta1}$::GBP) induced segregation. Maximum z-projection at establishment (top), maintenance phase (bottom), (n = 3).

Scale bars, 5 µm (A-D, J), 2.5 µm (E-G).

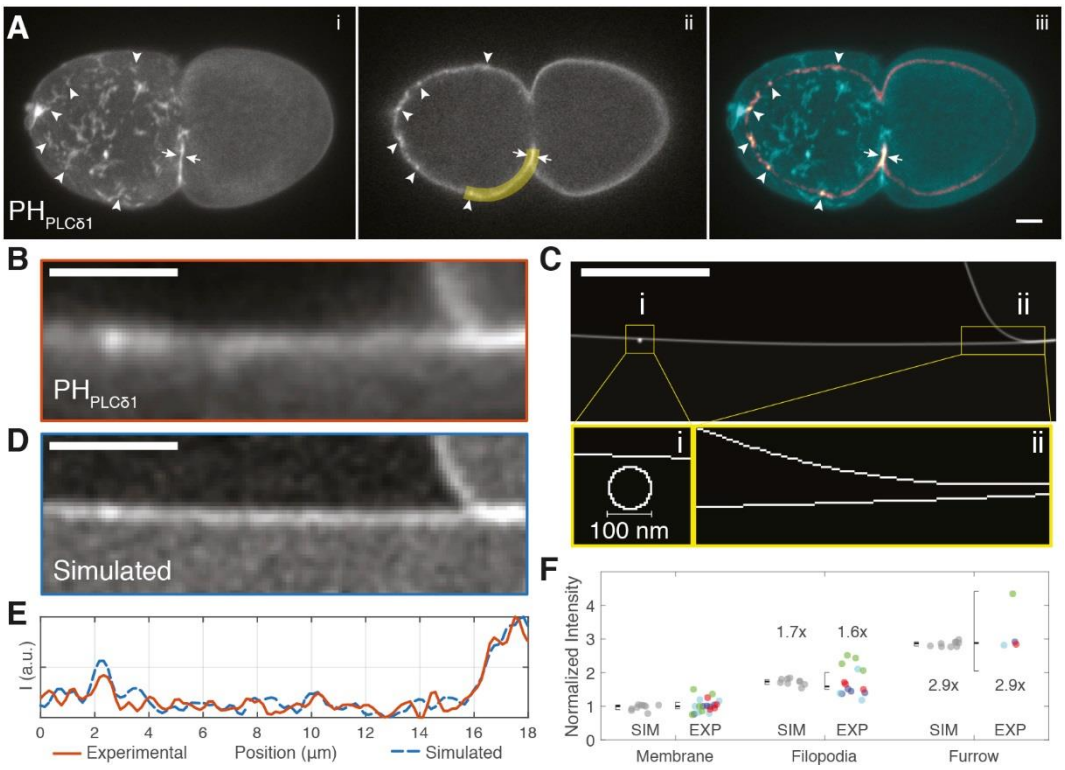

Figure 4. Bulk membrane accumulation quantitatively accounts for observed cortical 'enrichment'.

(A) Maximum z-projection (i), single plane (ii), and overlay (iii) of an establishment phase embryo expressing mCherry::$PH_{PLC\delta1}$. Arrowheads mark visible accumulations of signal in a single plane that can be identified as cross-sections of membrane structures based on the z-projection. White arrows mark double membrane generated at the pseudocleavage furrow.

(B) Straightened cortical region of the experimental image taken along the yellow line in (Aii).

(C) A 5 nm/px model of our filopodia model of the image in (B), including a 100 nm diameter membrane tube (zoom, i) and a double membrane region at right (zoom, ii).

(D) Simulated image following convolution of (C).

(E) Plot of mean-normalized intensity along the membrane in the experimental (B, red) and simulated image (D, dashed blue).

(F) Quantification of fluorescence intensity of putative filopodia relative to single membranes and furrow regions in experimental and simulated images. Datapoints from individual embryos are color coded (n = 4), normalized to median values and shown alongside median-normalized data from simulated image replicates (n = 10). Median ± 95% CI indicated along with fold-change in median.

Scale bars, 5 μm.

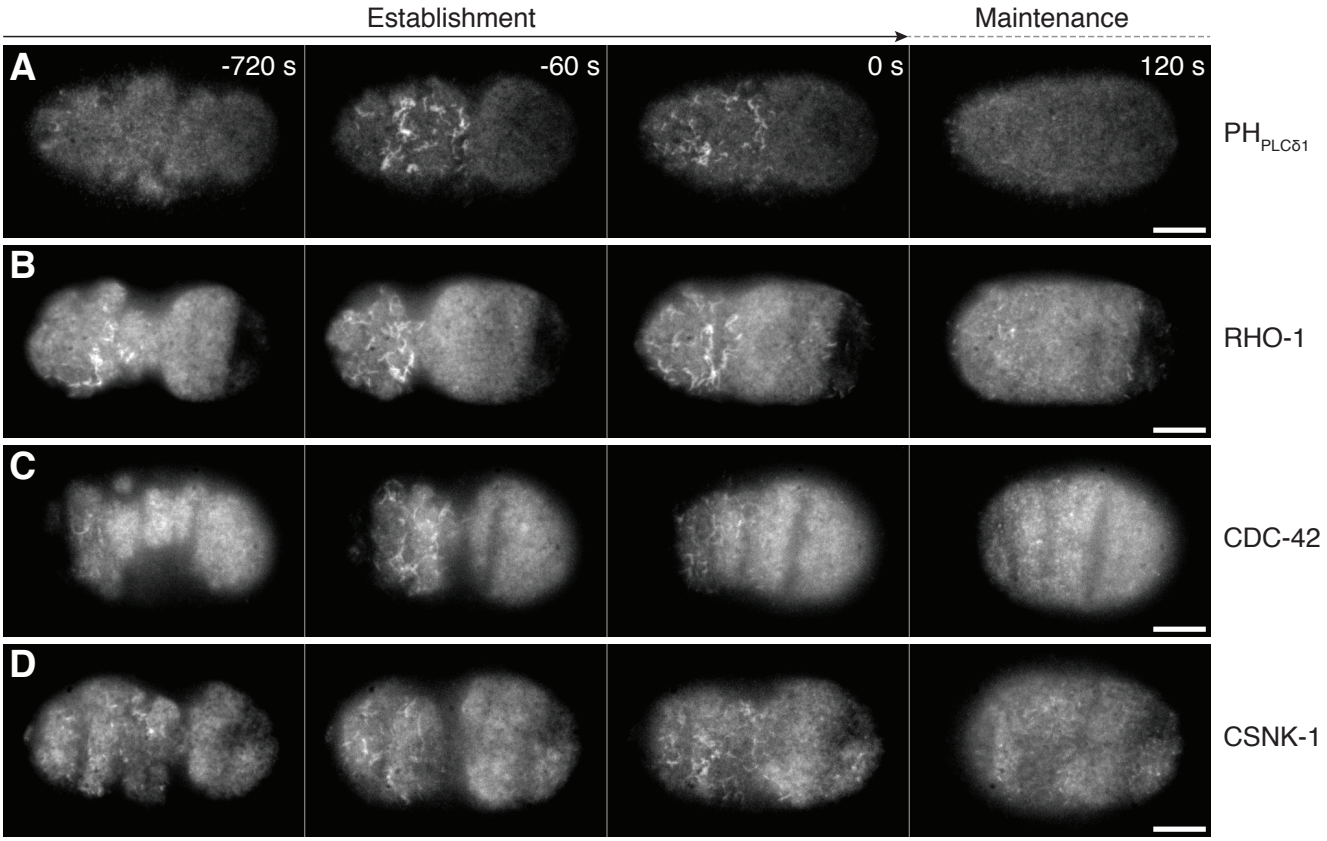

Figure S1. Diverse signaling molecules appear enriched in cortical structures. (A-D) HiLo microscopy images of mCherry::$PH_{PLC\delta1}$ (n>5) (A), GFP::RHO-1 (n = 2) (B), CDC-42::mCherry (n = 3) (C), and GFP::CSNK-1 (n = 2) (D) at the cell cortex are shown from early symmetry-breaking to maintenance phase. All accumulated during the polarity establishment phase which is associated with a dynamic, highly-contractile actomyosin cortex and anterior-directed actomyosin cortical flows, before peaking and then declining as the embryo transitions to the so-called polarity maintenance phase which corresponds roughly to prometaphase to anaphase (***Cuenca et al., 2003***; ***Munro et al., 2004***). Time (s) relative to the end of establishment phase. Scale bar, 10 um.

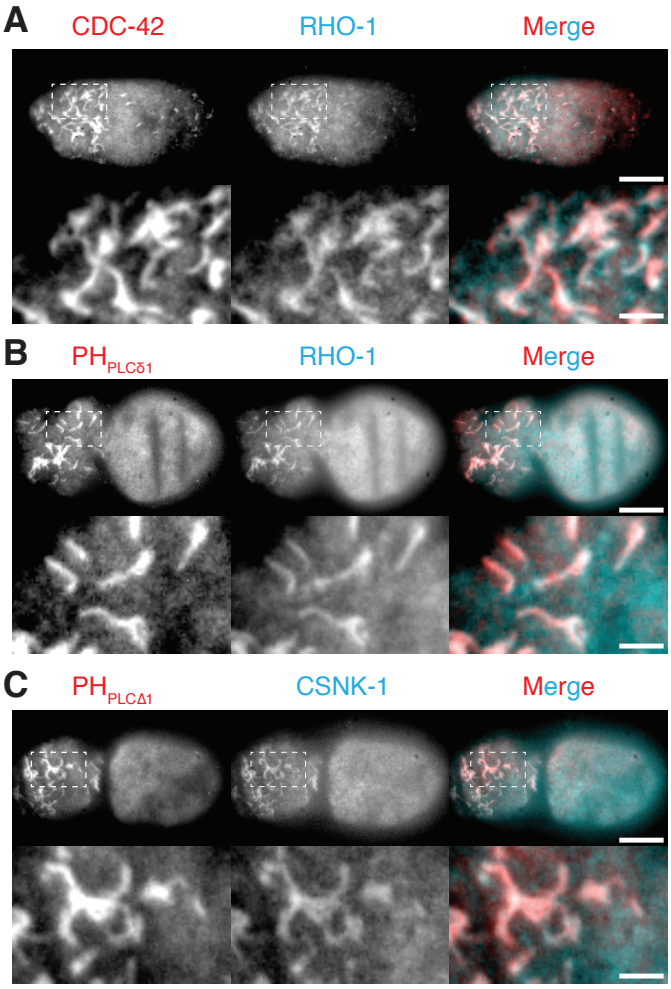

Figure S2. Colocalization of signaling molecules with the PIP_2 probe $PH_{PLC\delta1}$. **(A)** Sample image of surface of embryo co-expressing GFP::RHO-1 and mCherry CDC-42. Individual channels and merge shown with zoom of inset region to highlight structures. **(B)** As in (A), but GFP::RHO-1 with mCherry::$PH_{PLC\delta1}$. **(C)** As in (A), but GFP::CSNK-1 with mCherry::$PH_{PLC\delta1}$. Co-enrichment quantified in Figure 1B. Scale bars, 10 um.

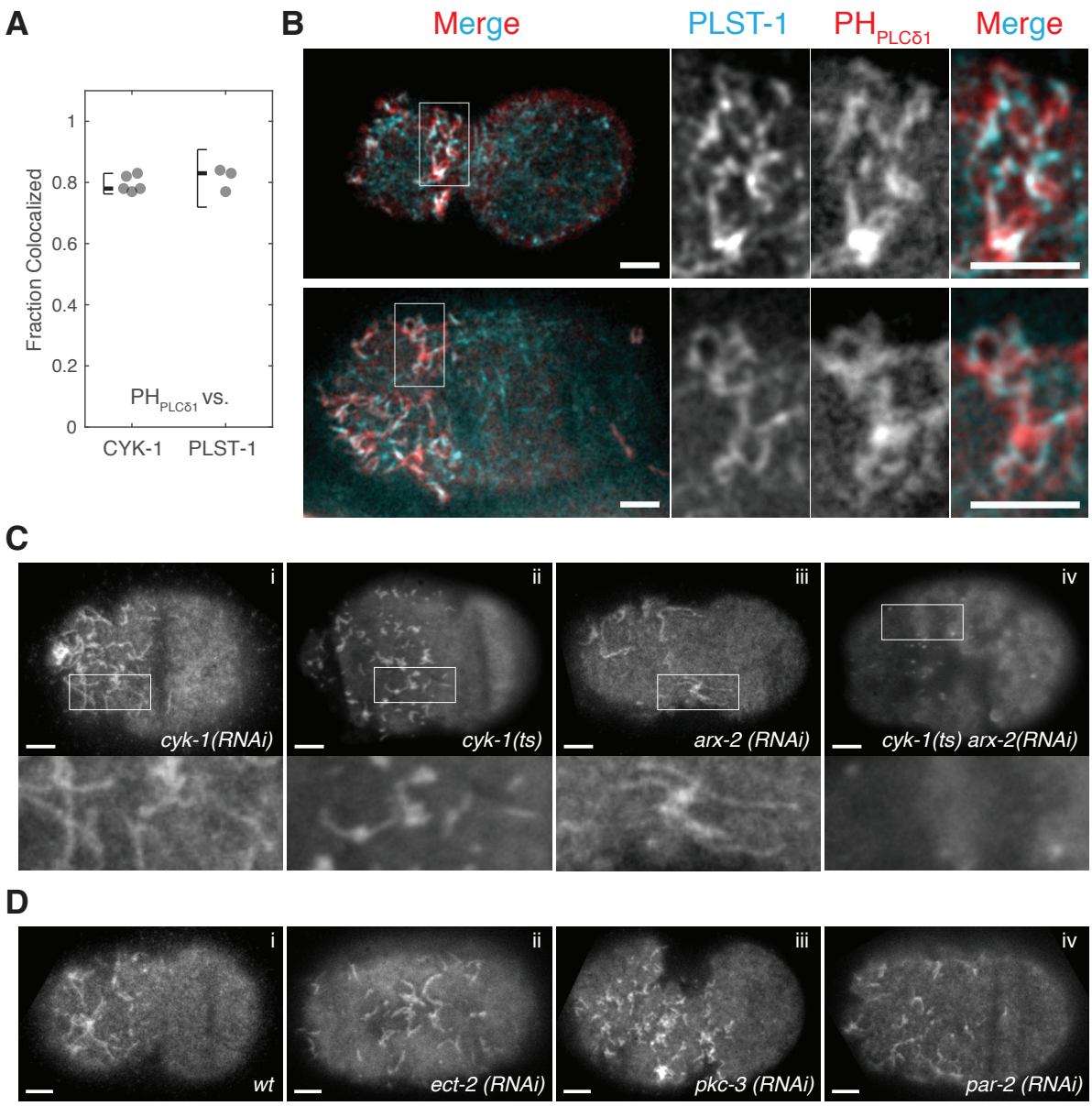

Figure S3. Filopodia are enriched in actin bundling proteins, require actin polymerization, and respond to polarity cues. **(A)** Fraction of selected $PH_{PLC\delta1}$-labeled structures that exhibit colocalized CYK-1 puncta at tips or enrichment in PLST-1. Datapoints from individual embryos shown. Median ± 95%CI indicated. **(B)** Cortical images of two embryos expressing PLST-1::GFP and mCherry::$PH_{PLC\delta1}$. Inset is marked and magnified on right showing merged and single channel images. **(C)** Disruption of both CYK-1 and ARX-2 lead to loss of filopodia like structures. mCherry (i,iii) or GFP (ii,iv) fusions to $PH_{PLC\delta1}$ persist when either ARX-2 or CYK-1 are disrupted on their own, but not when both are compromised. Insets magnified below to highlight filopodia structure. **(D)** Formation of filopodia is not affected when contractility is compromised by depletion of the RhoGEF, ECT-2, or when polarity is disrupted by depletion of PKC-3 or PAR-2 by RNAi. However, asymmetry of filopodia is reduced in all three cases consistent with their asymmetry requiring polarity. ECT-2 depletion compromises symmetry-breaking during the establishment phase (***Zonies et al., 2010***). Images shown reflect a timepoint of peak filopodial density just before relaxation of the cortex and filopodial disassembly. Scale bars, 5 μm.

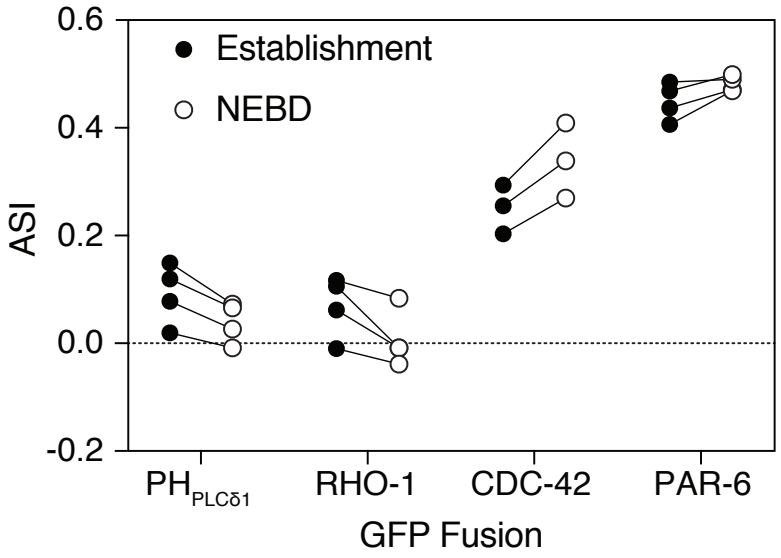

Figure S4. Asymmetry in membrane concentration from midplane images. Membrane fluorescence profiles were traced from midplane images of embryos expressing the indicated GFP fusions at mid-establishment (5 min pre-NEBD) or mid-maintenance phase (NEBD). For each embryo the asymmetry index (ASI) was calculated at each timepoint from the extracted profiles. Note asymmetry of both $PH_{PLC\delta1}$ and RHO-1 is low at establishment phase and is reduced further at maintenance phase when filopodia dissipate, consistent with filopodia contributing to weak apparent asymmetry during the establishment phase. By contrast, CDC-42 exhibits moderate asymmetry during establishment when anterior filopodia are high, but its asymmetry increases further by NEBD, when filopodia dissipate. For reference, the polarity protein PAR-6, which is not prominently enriched in these structures due to association with PAR-3 clusters, is highly polarized at both time points. Together these data suggest that filopodia-like structures, despite being highly asymmetric, do not contribute significantly to overall polarity in membrane concentrations.

Table 1. *C. elegans* strains used in this work.

Strain	Genotype	Source
ACR004	*cyk-1(ges1[cyk-1::eGFP + LoxP unc-119 (+) LoxP] III; unc-119 (ed3) III; ltIs44pAA173; [pie-1p::mCherry::PH(PLC1delta1) + unc-119(+)] V*	This work
ACR010	*plst-1(ges2[plst-1::eGFP + LoxP unc-119 (+) LoxP] IV; unc-119 (ed3) III ; ltIs44pAA173; [pie-1p::mCherry::PH(PLC1delta1) + unc-119(+)] V*	This work
AD189	*unc-119(ed3) III; asIs2[unc-119(+) + ppie-1::GFP::egg-1]*	CGC, ***Kadandale et al.*** (***2005***)
FT204	*unc-119(ed3) III; xnIs87[Psyn-4::GFP:::syn-4::syn-4 3'UTR + unc-119(+)]*	CGC
JA1354	*unc-119(e2498) III; weIs12[unc-119(+) + pie-1p::GFP::csnk-1]*	CGC, ***Panbianco et al.*** (***2008***)
JCC146	*cyk-1(or596ts); unc-119(ed3); ltIs38 [pAA1; pie-1/GFP::PH(PLC1delta1)III; unc-119 (+)]; ltIs37 [pAA64; pie-1/mCherry::his-58; unc-119 (+)]IV*	***Jordan et al.*** (***2016***)
KK1248	*par-6(it310[par-6::gfp]) I*	CGC, Ken Kemphues
NWG0045	*unc-119(ed3)III; crkIs16[mex-5p::mKate::iLiD::nym-2 3'UTR + unc-119(+)]*	This work
OD58	*unc-119(ed3) III; ltIs38[pAA1; pie-1::GFP::PH(PLC1delta1) + unc-119(+)]*	CGC, ***Audhya et al.*** (***2005***)
OD70	*unc-119(ed3) III; ltIs44pAA173; [pie-1p-mCherry::PH(PLC1delta1) +unc-119(+)] V*	CGC, ***Kachur et al.*** (***2008***)
SA115	*tjIs1[pie-1::GFP::rho-1 + unc-119(+)]*	CGC, ***Motegi and Sugimoto*** (***2006***)
SWG1	*mex-5p::Lifeact::mKate2*	***Reymann et al.*** (***2016***)
SWG5	*plst-1(ges2[plst-1::eGFP + LoxP unc-119 (+) LoxP] IV; unc-119 (ed3) III)*	***Reymann et al.*** (***2016***)
SWG19	*cyk-1(ges1[cyk-1::eGFP + LoxP unc-119(+) LoxP) III; unc-119(ed3) III.*	***Reymann et al.*** (***2016***)
TH159	*ddls46[WRM0625bA11 GLCherry::cdc-42;Cbr-unc-119(+)]*	***Rodriguez et al.*** (***2017***)
TH220	*unc-119(ed3)III; ddIs86[pie-p1::LifeAct::GFP;unc-119(+)]*	***Redemann et al.*** (***2010***)
WS5018	*cdc-42(gk388) opIs295[cdc-42p::GFP::cdc-42(genomic)::cdc-42 3'UTR + unc-119(+)] II.*	CGC, ***Neukomm et al.*** (***2014***)

Movie 1. Timelapse video of the surface of a permeabilized embryo expressing $PH_{PLC\delta1}$::GFP (middle, cyan) and stained with FM4-64 (left, red). Scale bar, 2.5 µm. Elapsed time (sec). See related Figure 1F.

Movie 2. Timelapse video of filopodia extending into the pseudocleavage furrow in an embryo expressing CYK-1::GFP and mKate$_{myr}$. Scale bar, 5 µm. Elapsed time (mm:ss) shown. See related Figure 2A.

Movie 3. Timelapse video of dynamic filopodia on the surface of an embryo expressing CYK-1::GFP and $_{PLC\delta1}$::mCherry. Scale bar, 5 µm. Elapsed time (sec) shown. See related Figure 2D.

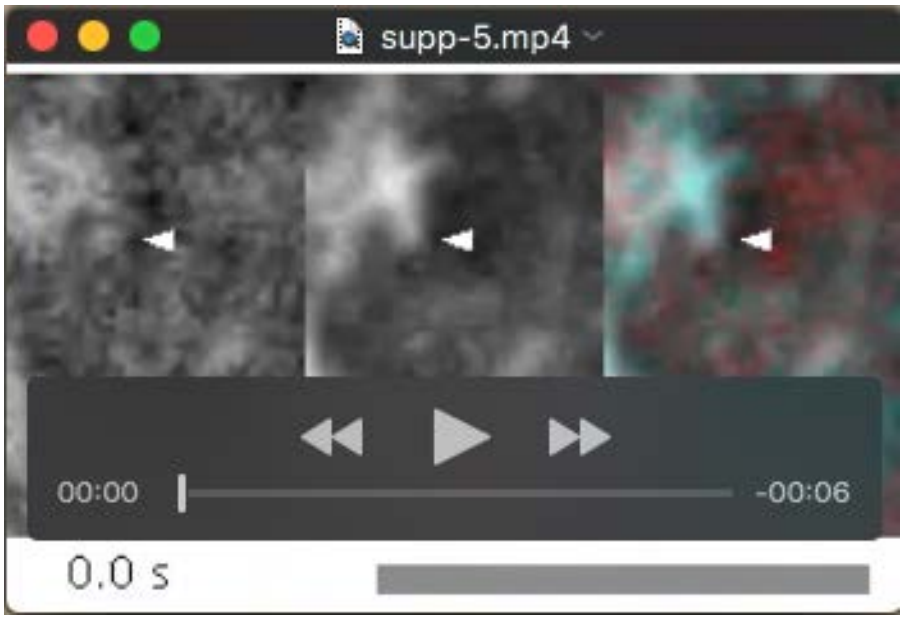

Movie 4. Timelapse video of an extending filopodium labeled with LifeAct::GFP and $_{PLC\delta1}$::mCherry on the surface of a one-cell embryo. Elapsed time (sec) shown. Scale bar, 5 µm. See related Figure 2F.

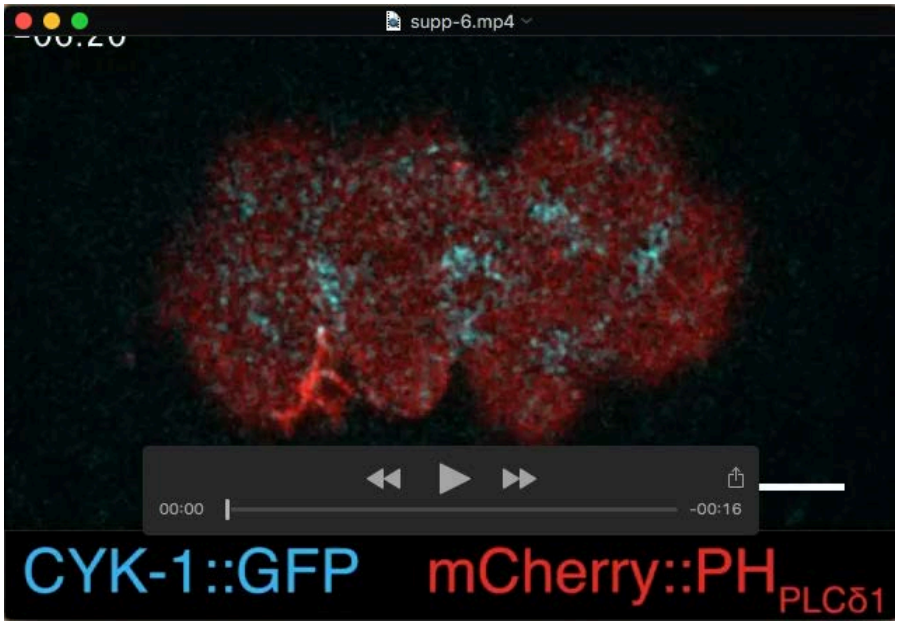

Movie 5. Timelapse video of the surface of an embryo expressing CYK-1::GFP and $PH_{PLC\delta1}$::mCherry by confocal microscopy showing the appearance, accumulation, segregation and dissipation of filopodia. Elapsed time shown (mm:ss). Scale bar, 5 µm. See related Figure 2K.

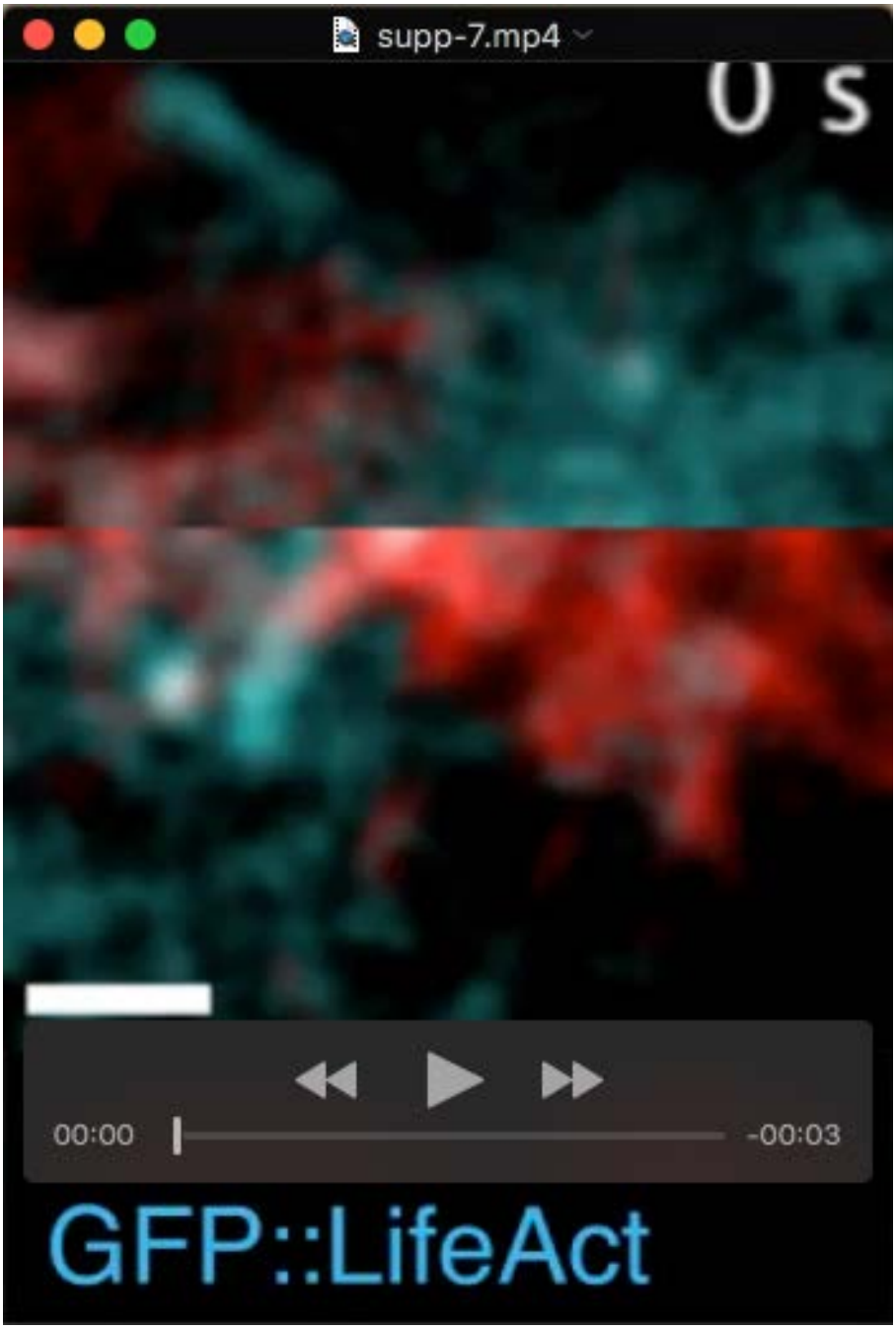

Movie 6. Timelapse video of two filopodia labeled with LifeAct::mKate (red) and LifeAct::GFP (cyan) corresponding to straightened filopodia shown in Figure 3E. Note lag of LifeAct::mKate signal relative to LifeAct::GFP yielding a cyan tip followed by a red tail. Elapsed time shown (sec). Scale bar, 2.5 µm. See related Figure 3F-G.

Journal of Cell Science • Supplementary information

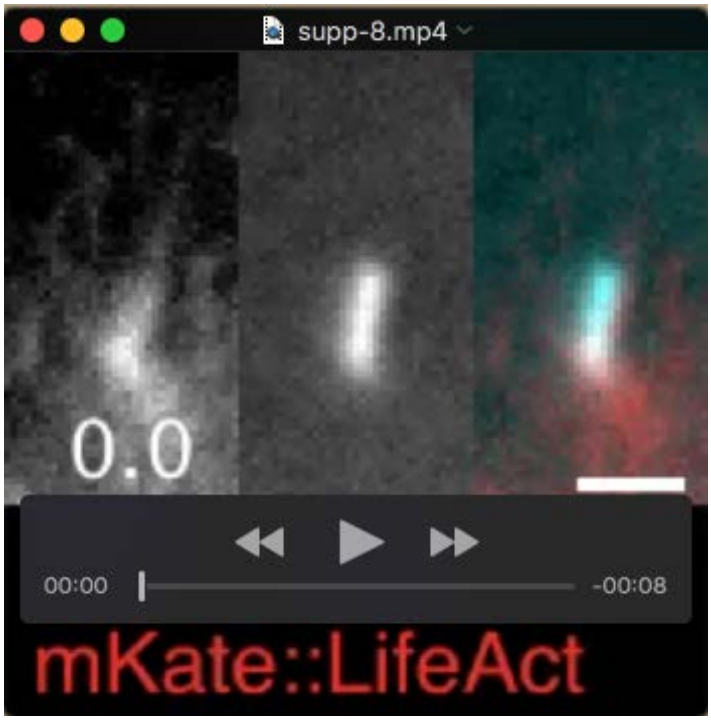

Movie 7. Timelapse video of cytoplasmic actin comet labeled with LifeAct::mKate (red) and LifeAct::GFP (cyan). Note lag of LifeAct::mKate signal relative to LifeAct::GFP yielding a cyan tip followed by a red tail. Elapsed time shown (sec). Scale bar, 2.5 μm. See related Figure 3G-H.